Supporting Information J. Electrochem. Sci. Technol., 2022, 13(4), 438-452

Rate Capability of $LiFePO_4$ Cathodes and the Shape Engineering of Their Anisotropic Crystallites

Alexander Bobyl[1]*, Sang-Cheol Nam[2], Jung-Hoon Song[2], Alexander Ivanishchev[2,3], and Arseni Ushakov[3]

[1]*Division of Solid State Physics, Ioffe Institute, Politekhnicheskaya Str. 26, St. Petersburg, Russian Federation (194021)*
[2]*Resarch Institute of Industrial Science and Technology RIST, POSCO Global R&D center, 100, Songdogwahak-ro, Yeonsu-gu, Incheon, South Korea (21985)*
[3]*Institute of Chemistry, Saratov State University, Astrakhanskaya Str. 83, Saratov, Russian Federation (410012)*

Content

1. XRD Volume-weighted length of ellipsoid and cuboid columns

The volume-averaged particle size is defined as the ratio of the fourth moment of the distribution function of the linear (observed) size L to the third moment [1]

$$\bar{L}_V = \frac{\overline{L^4}}{\overline{L^3}} = \frac{\int_0^\infty p(L)L^4 dL}{\int_0^\infty p(L)L^3 dL}, \quad \text{(S1)}$$

where $p(L)$ is the particle distribution function. If the distribution function of N particles is given by the histogram $p_i(L_i)$, then the integration is replaced by the summation over its i-th steps [1]

$$\bar{L}_V = \frac{\overline{L^4}}{\overline{L^3}} = \frac{\sum_{i=1}^{N} L_i^4 p_i(L_i)}{\sum_{i=1}^{N} L_i^3 p_i(L_i)}. \quad \text{(S2)}$$

The crystallite size $\bar{L}_{Vc}$, obtained by the XRD method, is the averaging of the column lengths over their volume, which are shown in Fig. 1 and which are located perpendicular to the reflecting planes [2].

*E-mail address: bobyl@theory.ioffe.ru

DOI: https://doi.org/10.33961/jecst.2022.00248

$$\bar{L}_{V1} = \frac{1}{V}\int M_1\, dv \quad \text{(S3)}$$

For some crystallite forms, these sizes are related by a simple relationship

$$\bar{L}_{i\,XRD} \equiv \bar{L}_{Vi} = k\bar{L}_V = k\bar{L}\left(\frac{7}{2}ln^2\sigma\right), \quad \text{(S4)}$$

where the last equality is given for the lognormal distribution of linear particle sizes with an average value $\bar{L}$ and variance σ[3], aspect ratio k = 1 for a cuboid (rectangular parallelepiped), k = ¾ for a sphere [4] and for an ellipsoid shown in Fig. S1.

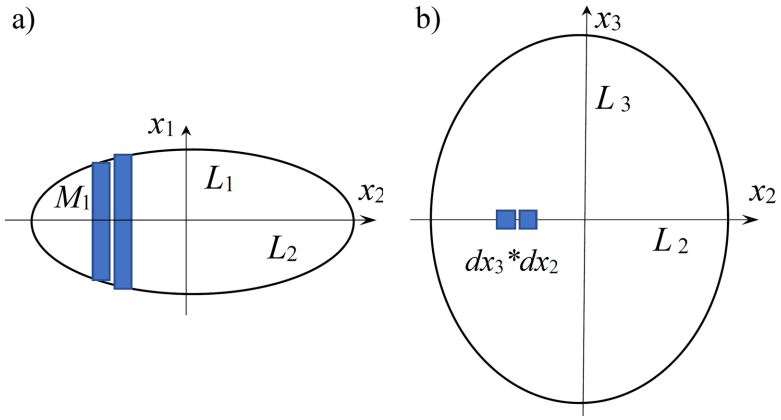

Fig. S1. An ellipsoid with axes L_1, L_2, L_3, its sections by the plane (a) x_1, x_2 at $x_3 = 0$ and (b) x_2, x_3 at $x_1 = 0$. For example, projections of some columns of length M_1 on x_1, x_2 plane and their cross-section $dx_3 * dx_2$ on x_3, x_2 plane are shown.

The column weighted size of ellipsoid along x_1 is determined by integrating the length of columns M_1 along this axis over ellipsoid volume

$$\bar{L}_{V1} = \frac{1}{V}\int M_1\, dv = \frac{1}{\frac{1}{6}\pi L_1 L_2 L_3}\iiint M_1 dx_3 dx_2 dx_1 = \frac{6}{\pi L_1 L_2 L_3}\int_{-L_3/2}^{L_3/2} dx_3 \int_{-\acute{L}_2/2}^{\acute{L}_2/2} M_1^2 dx_2 \ , \quad \text{(S5)}$$

where in the last expression $\acute{L}_2$ is the value of the ellipse axis in the plane x_1, x_2 at $x_3 \neq 0$.

From the ellipse equation,

$$\frac{x_2^2}{\left(\frac{\acute{L}_2}{2}\right)^2} + \frac{\left(\frac{M_1}{2}\right)^2}{\left(\frac{\acute{L}_1}{2}\right)^2} = 1 \quad \text{(S6)}$$

an expression for M_1 is obtained

$$M_1 = 2\frac{\acute{L}_1}{\acute{L}_2}\sqrt{\left(\frac{\acute{L}_2}{2}\right)^2 - x_2^2}; \quad \text{(S7)}$$

the integration $\int_{-M_1/2}^{M_1/2} dx_1 = M_1$ is carried out, since M_1 does not depend on x_1. Using expression (3), one can carry out integration over x_2

$$L_{V1} = \frac{6}{\pi L_1 L_2 L_3}\int_{-\frac{L_3}{2}}^{\frac{L_3}{2}} dx_3 \int_{-\frac{\acute{L}_2}{2}}^{\frac{\acute{L}_2}{2}} 4\frac{\acute{L}_1^2}{\acute{L}_2^2}\left[\left(\frac{\acute{L}_2}{2}\right)^2 - x_2^2\right] dx_2 = \frac{4}{\pi L_1 L_2 L_3}\int_{-\frac{L_3}{2}}^{\frac{L_3}{2}} \acute{L}_1^2\, \acute{L}_2\, dx \quad \text{(S8)}$$

Let us determine the dependence of $\acute{L}_1$ and $\acute{L}_2$ on the coordinate x_3. Similarly with (S7), one can obtain

$$\acute{L}_1 = 2\frac{L_1}{L_2}\sqrt{\left(\frac{L_3}{2}\right)^2 - x_3^2} \quad \acute{L}_2 = 2\frac{L_2}{L_3}\sqrt{\left(\frac{L_3}{2}\right)^2 - x_3^2} \text{ (S9)}$$

Substituting (S9) into (S8) we get

$$L_{V1} = \frac{2L_1}{\pi}\int_{-1}^{1}\left(1-\left(\frac{x_3}{\frac{L_3}{2}}\right)^2\right)\left(\sqrt{1-\left(\frac{x_3}{\frac{L_3}{2}}\right)^2}\right)d\frac{x_3}{\frac{L_3}{2}} = \frac{2L_1}{\pi}\int_{-1}^{1}(1-x^2)^{\frac{3}{2}}dx = \frac{2L_1}{\pi}\frac{3\pi}{8} = \frac{3}{4}L_1, \text{ (S10)}$$

where the variable of integration was changed and it turned out that the calculations led to a tabular integral.

That is, the aforementioned aspect ratio value for an ellipsoid completely coincides with the value for a sphere, which can also be obtained using the approach described here.

Expression (S10) can be verified by the Wolfram Mathematica program

In[1]:= f[x_]:=(Subscript[L, 3]^2/4-x^2)^1.5

L_{V1}= (32*Subscript[L,1])/(\[Pi]*Subscript[L,3]^4)*Integrate[f[x],{x,-(Subscript[L, 3]/2),Subscript[L, 3]/2}]

Out[2]= 0.75*Subscript[L,1] (S11)

References

[1] M. Leoni and P. Scardi, *J. Appl. Cryst.*, **2004**, *37(4)*, 629-634.
[2] E. F. Bertaut, *Acta Crystallogr.*, **1950**, *3(1)*, 14-18.
[3] W. C. Hinds, Chapter 4 Particle size statistics, *Aerosol Technology: Properties, Behavior, and Measurement of Airborne Particles*, New York, Wiley, **1982**.
[4] B. E. Warren, Chapter 13, *X-ray Diffraction,* New York, Dover Publications, **1990**, 147.

2. Rate capability as one of the most important operational parameters of chemical current sources

The significant dependence of their electrical capacity on the charging or discharge rate should be considered one of the inherent features of electrochemical power sources (EPSs). The high charging and discharge rates are critical for some applications [1]. The operation of an EPS is accompanied by charge transfer across the interface between the ion conductor and the electron conductor (Faradaic reactions), through other conductor interfaces and along the phase interface, as well as the transfer of ions or electrons inside each conductor, according to the direction of the electric current. The transfer of charge across the boundary of the conductors of ions and electrons is often accompanied by successive chemical and phase transformations, as well as a physical process [2,3].

In a number of cases, the redistribution of charge carriers near the interphase boundaries without charge transfer through the interface itself (electric double layer; almost 100% responsible for the electrical capacity of supercapacitors) is predominant [4]. The decrease in the capacity, as well as the completeness of the process, with an increase in current load is associated with a limited speed of the steps of the process occurring in an EPS [2]. To each step can be assigned its own characteristic time. Occasionally, one can single out in a succession of steps the slowest one, with the longest characteristic time, which will be a rate-limiting step [5].

Modeling the dependence of the capacity of the most popular lithium-ion batteries today on the rate of charge or discharge is of considerable present interest. The classical model of M. Doyle and J. Newman [6] suggests of the stages of lithium-ion diffusion play a significant role in the filling by the liquid electrolyte of the pores in the electrode and in the solid phase of the active material, as well as in the ohmically-dominated reaction. Depending on the characteristic time of which stage predominates, one of three simple models can be applied, which correspond to limited diffusion in the solution phase, limited diffusion in the solid phase, or limited rate of the

electrochemical reaction itself. If the characteristic times of the steps are close, simple models are no longer applicable. For commercial cylindrical batteries, M. J. Lain and E. Kendrick [7] demonstrated the predominance of these limiting steps in exposure to high power pulses, with the anode is also coated with lithium in the process.

C. Heubner et al. suggested a limiting role for the diffusion of lithium ions in the pores of the electrode composite [8,9] and used the term "diffusion-limited C-rate" (DLC) to denote the limiting charging or discharge rate, above which a sharp decrease in electrical capacity is observed. The authors took into account several possible factors that affect not so much the electrical capacity of the active material as the electrical capacity of the entire electrode composite, which includes a binder and electrically conductive additives, a current collector, and an electrolyte that fills the pores of the composite. In [10], authors consider the advantages and disadvantages of physical and semi-empirical models for modeling the limitations in the behavior of electrode materials.

Experimentally, D. Parikh et al. [11,12] established a correlation of the mass load, porosity, and charge velocity with the specific capacity of the electrode material. F. Wang and M. A. Tang [13] offered a simple model for predicting the speed characteristics of batteries, in which the limiting factor in charging (discharging) of a battery is electrolyte transport. They consider whether or not the two-phase mechanism of intercalation and deintercalation of lithium ions characterize the electrode material. K. S. Mayilvahanan et al. pay detailed attention to how the tortuosity of pores affects the behavior of the electrode material [14].

It should be understood that any stage of the process in an EPS has its own specifics. The authors of review [15] consider the complete list of features that limit the charging and discharge rates, and they propose detailed requirements for materials that provide fast charging. The diffusion of lithium ions in the active material is the main factor limiting the charging rate. In the case of anode materials, the particle size becomes an essential factor in providing a fast charging if the diffusion is not fast enough. The particle morphology becomes another important factor for active materials with strong diffusion anisotropy, such as layered compounds. It requires a particular electrode microstructure with low tortuosity coefficients and optimized porosity, balancing electronic and ionic conductivity. A slightly different behavior is observed for the cathode. In the case of cathode materials, the change in the chemical diffusion coefficients of Li^+ and their crystal structure and phase changes most strongly affect the rate of the process [15,16]. The transfer in the bulk of the liquid electrolyte plays a less important role but is essential for the anode. In addition, the compatibility of the electrolyte with active materials is of interest since degradation occurs on both sides of the anode and cathode [15,17].

At high currents and a developed surface of active materials or additives, the effect of the capacitance of the electrical double layer is significant. The use of appropriate models (for example, A. Kornyshev [18]) is crucial for characterizing the behavior of supercapacitor electrodes.

Models represented by equations in which the values of one of the parameters vary depending on the limiting step are attractive. For example, the authors of [19,20] propose an analytical model, according to which the decrease in the capacitance of the current source in comparison with the limiting of maximum capacitance is proportional to $(R\tau)^n(1-e^{-(R\tau)^{-n}})$, where R is the current normalized to the capacitance; τ and n, are, respectively, the characteristic time of a stage and the exponent dependent on the limiting step. This model is attractive due to its versatility.

Formula proposed by the authors [20]:

$$\frac{Q}{M} = Q_M[1-(R\tau)^n(1-e^{-(R\tau)^{-n}})] \quad \text{(S12)}$$

can be interpreted as follows: the specific capacity $\frac{Q}{M}$ reached in the course of time $\frac{1}{R}$ is equal to the limiting specific capacity Q_M, multiplied by the probability $[1-(R\tau)^n(1-e^{-(R\tau)^{-n}})]$ of implementation of the process responsible for the buildup or decrease in capacity. Then the subtrahend $\left\{(R\tau)^n(1-e^{-(R\tau)^{-n}})\right\}$ has the meaning

of the probability of the process not being implemented due to the limited rate of *one* limiting step [21]. In this case, the role of a limiting stage is determined by the following parameters: the characteristic period (time) τ and the exponent n.

Let us develop this model for the case when it is impossible to identify one limiting stage in two directions.

2.1 Parallel process steps

If we consider that the charge accumulation in the electrode is possible due to N parallel processes, the probability of failure of the whole process will be equal to the product of the probabilities of failure of each of the parallel components of the process. Therefore, the formula for the specific capacity of the electrode material, obtained during a given time can also be compiled by analyzing the probabilities of events [21]:

$$\frac{Q}{M} = Q_M\left[1 - \Pi_{i=1}^{N}(R\tau_i)^{n_i}\left(1 - e^{-(R\tau_i)^{-n_i}}\right)\right]. \quad \text{(S13)}$$

It is assumed that, in the case of the limiting diffusion step in Faradaic processes with electrode materials in batteries, n = 0.5, and τ_d is the characteristic time. If the charging of the electric double layer charge in supercapacitor materials is the limiting step, n = 1, and τ_{el} is the characteristic time [20]. The mixed parallel influence of these two components is represented by the expression:

$$\frac{Q}{M} = Q_M\left\{1 - \left[(R\tau_d)^{0.5}\left(1 - e^{-(R\tau_d)^{-0.5}}\right)\right] \cdot \left[(R\tau_{el})\left(1 - e^{-(R\tau_{el})^{-1}}\right)\right]\right\}. \quad \text{(S14)}$$

This model assumes the flow of charge carriers in parallel through the capacitor (the model of a dense electric double layer) and an element with distributed parameters (the Warburg element is a model of the diffusion stage limiting the rate of the Faradaic process). It is similar to using one of the equivalent circuit fragments to analyze the electrochemical impedance in which these elements are connected in parallel to form a circuit [22]:

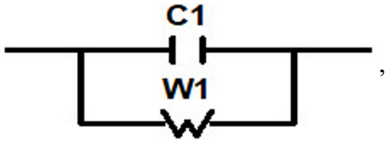

,

where C1 — the capacitor, W1 — the Warburg element.

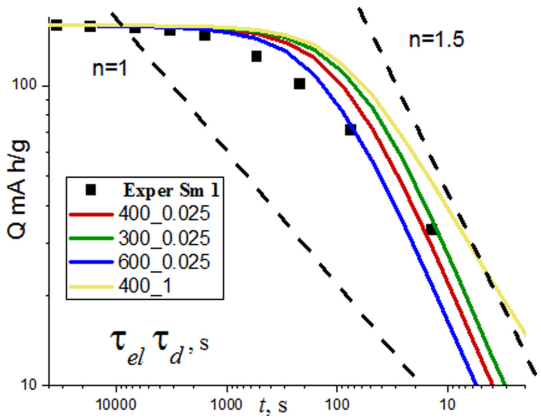

Fig. S2. Calculations by integration over the crystallite (3) and summation over their 3D distribution.

In this study, we apply the model (S14) to a physically small volume of a crystallite of solid electrode material, rather than to an electrode or an electrochemical circuit as this was done in [20] by using formula (S12). The characteristic of the electrode is obtained by integrating formula (S14) over the volume of crystallites and summing over their 3D distribution (Fig. S2). It demonstrates that the model cannot explain the slope of the

specific capacitance-vs.-discharge time curve for a fast process (at short times). The slope of the corresponding section is close to 1.5 for different values of the variable parameters. At the same time, the experimental points are located with a slope close to unity.

2.2 Serial steps of the process

If we consider that charge accumulation in the electrode is possible due to *N* successivel processes, the probability of the whole process will be equal to the product of the probabilities of each of the successive components of the process. Therefore, the formula for the specific capacity of the electrode material obtained during a given time can also be compiled by analyzing the probabilities of the events [21]:

$$\frac{Q}{M} = Q_M \cdot \Pi_{i=1}^{N}\left[1-(R\tau_i)^{n_i}\left(1-e^{-(R\tau_i)^{-n_i}}\right)\right]. \quad \text{(S15)}$$

If we consider the charging or discharge of the electrical double layer and the diffusion of ions as two successive components, then the influence of these components will be taken into account by the following expression:

$$\frac{Q}{M} = Q_M \cdot \left[1-(R\tau_d)^{0.5}\left(1-e^{-(R\tau_d)^{-0.5}}\right)\right] \cdot \left[1-(R\tau_{el})\left(1-e^{-(R\tau_{el})^{-1}}\right)\right] \quad \text{(S16)}$$

The model can be considered similar to the electrical circuit in which the capacitor and the Warburg element are series-connected [22]:

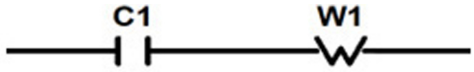

Application of this model (formula S16) to a physically small crystallite volume of the electrode material, followed by integration over the volume of crystallites and summation over their 3D distribution, gives better agreement with the experimental data (Fig. 6) in comparison with the use of formula (S14).

2.3 Recalculation of recharge time *t*

R is the rate of charging or discharge. It is expressed as the ratio of the specific current to the specific capacity: $R = \frac{I/m}{Q/m}$ [20]. To estimate the charging-discharge currents in our experiment, the theoretical specific capacitance was considered, so the values of *R* that must be taken in the simulation differ from those set by the ratio:

$$R = \frac{I/m}{Q/m} = \frac{(Q/m)theor}{Q/m} \quad \text{(S17)}$$

where $(Q/m)_{theor}$ is the theoretical specific capacity of the electrode material, mA·h·g^{-1}; Q/m is the practical specific capacity of the electrode material, mA·h·g^{-1}, at a current normalized to the theoretical capacitance, $C = \frac{I/m}{(Q/m)_{theor}}$. For $LiFePO_4$ $(Q/m)_{theor}$ = 169.89 mA·h·g^{-1}.

The results of recalculation of *C* to *R* are listed in the table for P2 sample.

C/ h^{-1}	0.1	0.2	0.5	1	2	5	10	20	50
R /h^{-1}	0.106	0.215	0.548	1.11	2.31	6.78	16.7	47.9	256

References

[1] Office of Electricity, *Potential benefits of high-power, high-capacity batteries*, United States Department of Energy, Washington, DC 20585, **2020**. https://www.energy.gov/oe/downloads/potential-benefits-high-power-high-capacity-batteries-january-2020

[2] V. S. Bagotsky, *Fundamentals of electrochemistry,* 2nd ed., John Wiley & Sons, **2006**.

[3] P. M. Biesheuvel and J. E. Dykstra, *Introduction to physics of electrochemical processes*, **2020**. http://www.physicsofelectrochemicalprocesses.com
[4] P. M. Biesheuvel, S. Porada, and J. E. Dykstra, *The difference between Faradaic and non-Faradaic electrode processes*, **2021**, arXiv:1809.02930v4.
[5] P. Atkins, J. De Paula, and J. Keeler, *Atkins' physical chemistry*, 11th ed., Oxford University Press, **2017**.
[6] M. Doyle and J. Newman, *J. Appl. Electrochem.*, **1997**, *27*, 846-856.
[7] M. J. Lain and E. Kendrick, *J. Power Sources*, **2021**, *493*, 229690.
[8] C. Heubner, M. Schneider, and A. Michaelis, *Adv. Energy Mater.*, **2020**, *10*, 1902523.
[9] C. Heubner et al., *J. Power Sources*, **2020**, *479*, 228704.
[10] C. Heubner et al., *Batte. Supercaps*, **2020**, *4(2)*, 268-285.
[11] D. Parikh, T. Christensen, and J. Li, *J. Power Sources*, **2020**, *474*, 228601.
[12] D. Parikh, *Understanding the limitations in battery components for improving energy density under extreme fast charging (XFC) conditions*, PhD diss., University of Tennessee, **2021**. https://trace.tennessee.edu/utk_graddiss/6504
[13] F. Wang and M. A. Tang, *Cell Reports Physical Science*, **2021**, *1(9)*, 100192.
[14] K. S. Mayilvahanan et al., *J. Electrochem. Soc.*, **2021**, *168(7)*, 070537.
[15] M. Weiss et al., *Adv. Energy Mater.*, **2021**, *11(33)*, 2101126.
[16] A. V. Ivanishchev et al., *Electrochim. Acta*, **2017**, *230*, 479-491.
[17] A. V. Ushakov et al., *Monatsh. Chem.*, **2019**, *150(3)*, 499–509.
[18] A. A. Kornyshev, *J. Phys. Chem. B.*, **2007**, *111(20)*, 5545-5557.
[19] S. O'Hanlon et al., *J. Electrochem. Soc.*, **2020**, *167(14)*, 140532.
[20] R. Tian et al., *Nat. Commun.*, **2019**, *10*, 1933.
[21] M. F. Triola, *Elementary statistics technology update*, 11th ed., Pearson Education, **2012**.
[22] V. F. Lvovich, Distributed impedance models, *Impedance spectroscopy: Applications to electrochemical and dielectric phenomena*, John Wiley & Sons, **2012**.

3. Verification of anisotropic crystallite size calculations of $LiFePO_4$ powders using Wolfram Mathematica 12

3D Lognormal distribution is compactly described by the matrix equation

$$f(\bar{L}) = \frac{1}{L_1 L_2 L_3 \sqrt{(2\pi)^3 \det K}} \exp\left[\left(-\frac{1}{2}\right)(\ln\bar{L} - \ln\bar{\bar{L}})^T K^{-1}(\ln\bar{L} - \ln\bar{\bar{L}})\right], \text{(S18)}$$

For the investigated powder, the quantities $\bar{\bar{L}}$, K, K^{-1}, det$K$ within the framework of the ellipsoidal model have the following experimental values

$$\bar{\bar{L}} = \begin{bmatrix} 92 \\ 108 \\ 160 \end{bmatrix} HM,\ K = \begin{bmatrix} 0.185 & 0.127 & 0.084 \\ 0.127 & 0.168 & 0.076 \\ 0.084 & 0.076 & 0.1225 \end{bmatrix}$$

In[18]: = K= ({{0.0185,0.127,0.084}, {0.127,0.168,0.076}, {0.084,0.076,0.1225}})
Inverse[K]
Out[19] = {{12.34628,-7.65054,-3.7195},{-7.65054,13.0155,-2.8288},{-3.71956,-2.8288,12.4688}}
Det[K]
Out[20] = 0.00119907 (S19)

Substitute in (S18) the values (S19)

$$f(L_1, L_2, L_3) = 1.039 \times 10^6 \times \frac{1}{(L_1 \times L_2 \times L_3)} \times \exp\left[-\frac{1}{2}\left(\ln\frac{\bar{L}}{\bar{\bar{L}}}\right)^T K^{-1} \ln\frac{\bar{L}}{\bar{\bar{L}}}\right]$$

$$= 2.9 \times 10^6 \times \frac{1}{(L_1 \times L_2 \times L_3)} \times \exp\left[-\frac{1}{2}\left(\ln\frac{\bar{L}}{\bar{\bar{L}}}\right)^T K^{-1} \ln\frac{\bar{L}}{\bar{\bar{L}}}\right]. \text{(S20)}$$

Using the 3D Lognorm function (S20) and the lognormal parameters of the anisotropic particle size distributions of $LiFePO_4$ powder (S19), we can compose a 3-dimensional i-bit matrix. For example, for $i = 4$, the calcu-

lation algorithm and the matrix have the following form

In[7]: $= f(L_1, L_2, L_3)$

$$= \text{NumberForm}\left[\text{Table}\left[\left\{1039000 \times \frac{1}{(L_1 \times L_2 \times L_3)}^{\left(0.5\left\{\left\{\text{Log}\left[\frac{L_1}{92}\right]\right\},\left\{\text{Log}\left[\frac{L_2}{108}\right]\right\},\left\{\text{Log}\left[\frac{L_3}{106}\right]\right\}\right\}\cdot\{7.6356,-0.66979,-4.8225\}\right.}\right.\right.$$

$$\left.\left.\left.\times e^{\{-0.66979,4.3569,-0.6296\},\{-4.8225,-1.6296,11.4668\}\cdot\left\{\left\{\text{Log}\left[\frac{L_1}{92}\right]\right\},\left\{\text{Log}\left[\frac{L_2}{108}\right]\right\},\left\{\text{Log}\left[\frac{L_3}{106}\right]\right\}\right\}}\right\},\right.\right.$$

$$\left.\left.\{L_1, 50, 350, 100\}\{L_2, 50, 350, 100\}\{L_3, 50, 350, 100\}\right]\text{//MatrixForm, 3}\right]$$

Out[7]//MatrixForm= $f(L_{1i}, L_{2i}, L_{3i}) =$

$$\begin{pmatrix} \begin{pmatrix}0.0174\\0.307\\0.0105\\0.000221\end{pmatrix} & \begin{pmatrix}0.00476\\0.18\\0.00873\\0.000232\end{pmatrix} & \begin{pmatrix}0.000435\\0.0234\\0.00134\\0.000396\end{pmatrix} & \begin{pmatrix}0.000483\\0.00328\\0.000209\\6.65\times10^{-6}\end{pmatrix} \\ \begin{pmatrix}0.0000115\\0.0685\\0.035\\0.00438\end{pmatrix} & \begin{pmatrix}7.08\times10^{-6}\\0.0901\\0.0655\\0.103\end{pmatrix} & \begin{pmatrix}9.41\times10^{-7}\\0.0171\\0.0146\\0.00257\end{pmatrix} & \begin{pmatrix}1.34\times10^{-7}\\0.00306\\0.00292\\0.000553\end{pmatrix} \\ \begin{pmatrix}1.66\times10^{-8}\\0.00148\\0.00266\\0.000762\end{pmatrix} & \begin{pmatrix}1.48\times10^{-8}\\0.00283\\0.00724\\0.00262\end{pmatrix} & \begin{pmatrix}2.35\times10^{-9}\\0.000638\\0.00192\\0.000776\end{pmatrix} & \begin{pmatrix}3.76\times10^{-10}\\0.000129\\0.000432\\0.000187\end{pmatrix} \\ \begin{pmatrix}7.5\times10^{-11}\\0.000398\\0.000164\\0.0000811\end{pmatrix} & \begin{pmatrix}8.61\times10^{-11}\\0.0000975\\0.000572\\0.000357\end{pmatrix} & \begin{pmatrix}1.53\times10^{-11}\\0.0000247\\0.00017\\0.000119\end{pmatrix} & \begin{pmatrix}2.63\times10^{-12}\\5.37\times10^{-6}\\0.0000413\\0.0000309\end{pmatrix} \end{pmatrix} \quad \text{(S21)}$$

The numerical value 0.0174 in the upper left corner of the matrix (S21) is proportional to the number of ellipsoidal particles with axes of 50×50×50 nm^3, i.e., spheres with a diameter of 50 nm, and in the lower right corner 0.0000309 - spheres with a diameter of 350 nm. To test the program, we will separately calculate the first number

In[21]:

$$= 1039000 \times \frac{1}{(50 \times 50 \times 50)}^{\left(0.5\left\{\left\{\text{Log}\left[\frac{50}{92}\right]\right\},\left\{\text{Log}\left[\frac{50}{108}\right]\right\},\left\{\text{Log}\left[\frac{50}{106}\right]\right\}\right\}\cdot\{7.6356,-0.66979,-4.8225\}\right.}$$

$$\left.\times e^{\{-0.66979,4.3569,-0.6296\},\{-4.8225,-0.6296,11.4668\}\cdot\left\{\left\{\text{Log}\left[\frac{50}{92}\right]\right\},\left\{\text{Log}\left[\frac{50}{108}\right]\right\},\left\{\text{Log}\left[\frac{50}{106}\right]\right\}\right\}}\right),$$

Out[21]={{0.0173917}}. (S22)

It is possible to carry out inverse calculations of the crystallite size distribution. For example, the first point on the L1 curve in Fig. 4 is calculated by the following program operations

mf = Table[f[L1, L2, L3], {L1, tL1}, {L2, tL2}, {L3, tL3}];

mf[[1]]//MatrixForm List[Total [Flatten[mf[[1]]]]] .

4. Calculation of rate capability using Wolfram Mathematica 12

4.1 Calculations and their verification

Using the charge-discharge model and take into account only the diffusion part of the relaxation time, the capacity averaged over unit columns of length M_1 along the crystallographic axis, for the capacity of a rectangular parallelepiped as a whole with sides L_1, L_2, L_3 has a simple form

$$Q_1(L_1, L_2, L_3) = L_2 \times L_3 \times q_0 \left\{ 1 - \left[\left(\frac{1}{t} \frac{L_1^2}{\pi^2 D} \right)^{0.5} \right] \left[1 - \exp\left(- \left(\left(\frac{1}{t} \frac{L_1^2}{\pi^2 D} \right)^{0.5} \right)^{-1} \right) \right] \right\}, \quad \text{(S23)}$$

For an ellipsoid, we obtain the following expression

$$Q_1(L_1, L_2, L_3) = q_0 \int_{-\frac{L_3}{2}}^{\frac{L_3}{2}} dx \int_{-\frac{\acute{L}_2}{2}}^{\frac{\acute{L}_2}{2}} \left\{ 1 - \left[\left(\frac{1}{t} \frac{M_1^2}{\pi^2 D} \right)^{0.5} \right] \left[1 - \exp\left(- \left(\left(\frac{1}{t} \frac{M_1^2}{\pi^2 D} \right)^{0.5} \right)^{-1} \right) \right] \right\} dx_2 \quad \text{(S24)}$$

where $M_1 = \sqrt{\frac{L_1^2}{4} - \frac{L_1^2}{L_3^2} x_3^2 - \frac{L_1^2}{L_2^2} x_2^2}$, $\acute{L}_2 = \frac{L_2}{L_3} \sqrt{\left(\frac{L_3}{2}\right)^2 - x_3^2}$.

Finally, we get

$$Q_1(L_1, L_2, L_3) = q_0 \int_{-\frac{L_3}{2}}^{\frac{L_3}{2}} dx_3 \int_{-\frac{L_2}{L_3}\sqrt{\left(\frac{L_3}{2}\right)^2 - x_3^2}}^{\frac{L_2}{L_3}\sqrt{\left(\frac{L_3}{2}\right)^2 - x_3^2}} \left\{ 1 - \left[\left(\frac{\frac{L_1^2}{4} - \frac{L_1^2}{L_3^2} x_3^2 - \frac{L_1^2}{L_2^2} x_2^2}{\frac{1}{t} \pi^2 D} \right)^{0.5} \right] \left[1 - \exp\left(- \left(\left(\frac{\frac{L_1^2}{4} - \frac{L_1^2}{L_3^2} x_3^2 - \frac{L_1^2}{L_2^2} x_2^2}{\frac{1}{t} \pi^2 D} \right) \right) \right) \right] \right\} dx_2 . \quad \text{(S25)}$$

Within the framework of the use of Wolfram Mathematica 12, it is possible to carry out integration over the area, in particular the ellipse

$$reg = \text{implicitRegion}[((x \times 2)/\text{L2})^2 + ((y \times 2)/\text{L3})^2 \le 1, \{x, y\}]; \quad \text{(S26)}$$

$$Q(L_1, L_2, L_3) = \iint_{\{y, x\} \in reg} \left\{ 1 - \left[\left(\frac{\frac{L_1^2}{4} - \frac{L_1^2}{L_3^2} x_3^2 - \frac{L_1^2}{L_2^2} x_2^2}{\frac{1}{t} \sqrt{6} D} \right)^{0.5} \right] \left[1 - \exp\left(- \left(\left(\frac{\frac{L_1^2}{4} - \frac{L_1^2}{L_3^2} x_3^2 - \frac{L_1^2}{L_2^2} x_2^2}{\frac{1}{t} \sqrt{6} D} \right)^{0.5} \right)^{-1} \right) \right] \right\} dydx . \quad \text{(S27)}$$

It can be simplified for given parameters D, t, for example, $D = 300$ nm^{2}s, $t = 360$ s

$$Q(L_1, L_2, L_3) = \iint_{\{y, x\} \in reg} \left\{ 1 - \left[\left(\frac{\frac{L_1^2}{4} - \frac{L_1^2}{L_3^2} y^2 - \frac{L_1^2}{L_2^2} x^2}{\frac{1}{360} \sqrt{6} 300} \right)^{0.5} \right] \left[1 - \exp\left(- \left(\left(\frac{\frac{L_1^2}{4} - \frac{L_1^2}{L_3^2} y^2 - \frac{L_1^2}{L_2^2} x^2}{\frac{1}{360} \sqrt{6} D} \right)^{0.5} \right)^{-1} \right) \right] \right\} dydx . \quad \text{(S28)}$$

Then you can get a 3-dimensional i-bit matrix $Q(L_{1i}, L_{2i}, L_{3i})$, similar to the 4-bit type (S21). A 12-bit one was used in the calculations. Next, get a 3-dimensional i-bit matrix $f(L_{1i}, L_{2i}, L_{3i})$ and the product of elements $f(L_{1i}, L_{2i}, L_{3i}) \times Q(L_{1i}, L_{2i}, L_{3i})$ and then the sum of all elements. This will be one number for the given values of the fitting and experimental parameters.

Let us illustrate the calculations of the rate capability from time t using the example of a 3-dimensional matrix of 4-discrete dimensions L_{1i}, L_{2i}, L_{3i}

{tL1, tL2, tL3} // MatrixForm

$$\begin{pmatrix} 20 & \frac{190}{3} & \frac{320}{3} & 150 \\ 30 & \frac{460}{3} & \frac{830}{3} & 400 \\ 30 & \frac{460}{3} & \frac{830}{3} & 400 \end{pmatrix}, \text{(S29)}$$

with 3D distribution function parameters: mean values $\bar{L}_1 = 15$ nm, $\bar{L}_1 = 20$ nm, $\bar{L}_1 = 30$ nm, variances $\sigma_i =$ 0.4, correlation coefficients $r_{ij} = 0.5$, correlation moment matrix K

K = {{0.16, 0.08, 0.08}, {0.08, 0.16, 0.08}, {0.08, 0.08, 0.16}}//MatrixForm

$$\begin{pmatrix} 0.16 & 0.08 & 0.08 \\ 0.08 & 0.16 & 0.08 \\ 0.08 & 0.08 & 0.16 \end{pmatrix} \text{(S30)}$$

and areas of integration with the program line

$$R1 = \text{ImplicitRegion}[((x \times 2)/20)^g + ((y \times 2)/30)^g \le 1, \{x, y\}]. \text{(S31)}$$

The three shapes used for these regions and the shapes of the corresponding crystallites are shown in Fig. S3. By using integration (S24) using 3-dimensional 4-discrete crystallite sizes (S29), a matrix (S32) of numerical capacitance values with $4^3 = 64$ elements can be obtained, calculated for $\tau = 100$ s, $D = 3$ nm^2/s, $t = 10$ s (360 C) and the sum of its elements is calculated, $178.95/q_0$.

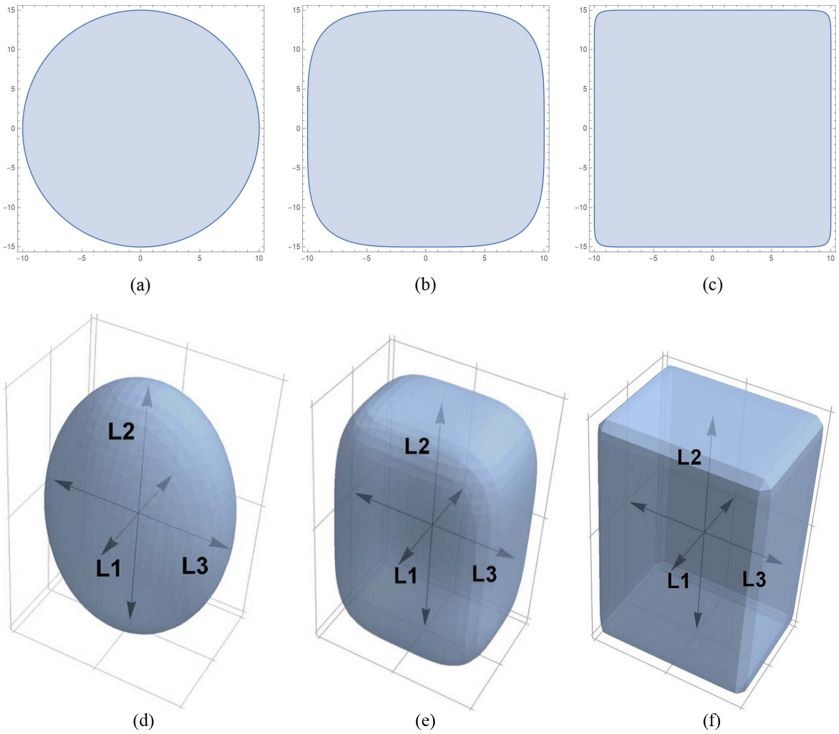

Fig. S3. Forms of integration regions specified by the line (S31) of the program, with axes along L_2, L_3 for three form parameters: (a) g=2, ellipse, (b) g=2, superellipse, (c) g=20, rectangle with rounded corners, and corresponding crystallite shapes: (d) g=2, ellipsoid, (e) g=2, superellipsoid, (f) g=20, cuboid with rounded edges (see below for more on the g shape parameter).

NumberForm[Q//MatrixForm,3]

	111	121	131	141	
111	″0.113″ ″0.579″ ″1.05″ ″1.51″	″0.579″ ″2.96″ ″5.34″ ″7.73″	″1.05″ ″5.34″ ″9.64″ ″13.9″	″1.51″ ″7.73″ ″13.9″ ″20.2″	141
112					142
113					143
114					144
211	″0.0497″ ″0.254″ ″0.458″ ″0.662″	″0.254″ ″1.3″ ″2.34″ ″3.38″	″0.458″ ″2.34″ ″4.22″ ″6.11″	″0.662″ ″3.38″ ″6.11″ ″8.83″	241
212					242
213					243
214					244
311	″0.0316″ ″0.161″ ″0.291″ ″0.421″	″0.161″ ″0.825″ ″1.49″ ″2.15″	″0.291″ ″1.49″ ″2.69″ ″3.88″	″0.421″ ″2.15″ ″3.88″ ″5.62″	341
312					342
313					343
314					344
411	″0.0231″ ″0.118″ ″0.213″ ″0.309″	″0.118″ ″0.605″ ″1.09″ ″1.58″	″0.213″ ″1.09″ ″1.97″ ″2.85″	″0.309″ ″1.58″ ″2.85″ ″4.11″	441
412					442
413					443
414					444

Total[Flatten[Q]] 178.95/q_0 for 10 s. (S32)

In the current calculations, 15 discrete size matrices were used with the number of elements $15^3 = 3375$. As an example (S32) shows the size indices for the nearest columns and rows, for example, 111 means that the upper left capacitance "0.113" is calculated for a crystallite from the (S29) matrix with dimensions along 3 of its axes 20×30×30 nm^3, taken from its left column, and 213 the capacitance "0.458" - with crystallite size 190/3×30×830/3 nm^3, etc. The result of a similar calculation for long times t = 60000 s (0.06 C) is the following matrix.

″4.46″ ″22.8″ ″41.2″ ″59.5″	″22.8″ ″117.″ ″210.″ ″304.″	″41.2″ ″210.″ ″379.″ ″549.″	″59.5″ ″304.″ ″549.″ ″793.″
″4.46″ ″22.8″ ″41.1″ ″59.5″	″22.8″ ″117.″ ″210.″ ″304.″	″41.1″ ″210.″ ″379.″ ″548.″	″59.5″ ″304.″ ″548.″ ″793.″
″4.46″ ″22.8″ ″41.1″ ″59.4″	″22.8″ ″116.″ ″210.″ ″304.″	″41.1″ ″210.″ ″379.″ ″548.″	″59.4″ ″304.″ ″548.″ ″793.″
″4.46″ ″22.8″ ″41.1″ ″59.4″	″22.8″ ″116.″ ″210.″ ″304.″	″41.1″ ″210.″ ″379.″ ″548.″	″59.4″ ″304.″ ″548.″ ″792.″

(S33)

Total[Flatten[Q]] = 14657. 1/q_0 for 60 000 s .

Using equation (S18), dimension matrix (S29), correlation moment matrix K (S30) the (S34) matrix of the 3D crystallite size distribution function can be obtained

$$\begin{pmatrix} \begin{pmatrix} "0.00109" \\ "0.000174" \\ "1.92\times10^{-7}" \\ "5.21\times10^{-10}" \end{pmatrix} & \begin{pmatrix} "0.000174" \\ "0.114" \\ "0.00255" \\ "0.0000454" \end{pmatrix} & \begin{pmatrix} "1.92\times10^{-7}" \\ "0.00255" \\ "0.00017" \\ "5.95\times10^{-6}" \end{pmatrix} & \begin{pmatrix} "5.21\times10^{-10}" \\ "0.0000454" \\ "5.95\times10^{-6}" \\ "3.19\times10^{-7}" \end{pmatrix} \\ \begin{pmatrix} "3.99\times10^{-8}" \\ "2.28\times10^{-6}" \\ "2.11\times10^{-8}" \\ "2.16\times10^{-10}" \end{pmatrix} & \begin{pmatrix} "2.28\times10^{-6}" \\ "0.533" \\ "0.0999" \\ "0.0067" \end{pmatrix} & \begin{pmatrix} "2.11\times10^{-8}" \\ "0.0999" \\ "0.0556" \\ "0.00736" \end{pmatrix} & \begin{pmatrix} "2.16\times10^{-10}" \\ "0.0067" \\ "0.00736" \\ "0.00149" \end{pmatrix} \\ \begin{pmatrix} "6.58\times10^{-12}" \\ "5.36\times10^{-9}" \\ "1.3\times10^{-10}" \\ "2.42\times10^{-12}" \end{pmatrix} & \begin{pmatrix} "5.36\times10^{-9}" \\ "0.0179" \\ "0.00877" \\ "0.00107" \end{pmatrix} & \begin{pmatrix} "1.3\times10^{-10}" \\ "0.00877" \\ "0.0128" \\ "0.00308" \end{pmatrix} & \begin{pmatrix} "2.42\times10^{-12}" \\ "0.00107" \\ "0.00308" \\ "0.00114" \end{pmatrix} \\ \begin{pmatrix} "5.57\times10^{-15}" \\ "2.58\times10^{-11}" \\ "1.17\times10^{-12}" \\ "3.24\times10^{-14}" \end{pmatrix} & \begin{pmatrix} "2.58\times10^{-11}" \\ "0.00049" \\ "0.000451" \\ "0.0000816" \end{pmatrix} & \begin{pmatrix} "1.17\times10^{-12}" \\ "0.000451" \\ "0.00123" \\ "0.00044" \end{pmatrix} & \begin{pmatrix} "3.24\times10^{-14}" \\ "0.000816" \\ "0.00044" \\ "0.00024" \end{pmatrix} \end{pmatrix} \quad \text{(S34)}$$

NumberForm[mf//Flatten,3][[1]]//Total = 1.000

When normalizing the sum of elements of a matrix to 1, the elements of this matrix do not depend on the fitting parameters τ, D and time t. Then we can obtain $Q(t)$, as an example for $t = 60000$ s, by multiplying the elements of the matrices (S34)and the matrix of their charge rate (S33) (the so-called Hadamard product), which is denoted as ($\overline{f} \cdot \overline{Q}$), and then summing them with a program line

$$\begin{pmatrix} \begin{pmatrix} "0.00486" \\ "0.00397" \\ "7.9\times10^{-6}" \\ "3.1\times10^{-8}" \end{pmatrix} & \begin{pmatrix} "0.00397" \\ "13.3" \\ "0.537" \\ "0.0138" \end{pmatrix} & \begin{pmatrix} "7.9\times10^{-6}" \\ "0.537" \\ "0.0644" \\ "0.00326" \end{pmatrix} & \begin{pmatrix} "3.1\times10^{-8}" \\ "0.0138" \\ "0.00326" \\ "0.000253" \end{pmatrix} \\ \begin{pmatrix} "1.78\times10^{-7}" \\ "0.0000519" \\ "8.67\times10^{-7}" \\ "1.28\times10^{-8}" \end{pmatrix} & \begin{pmatrix} "0.0000519" \\ "62." \\ "21." \\ "2.04" \end{pmatrix} & \begin{pmatrix} "8.67\times10^{-7}" \\ "21." \\ "21.1" \\ "4.04" \end{pmatrix} & \begin{pmatrix} "1.28\times10^{-8}" \\ "2.04" \\ "1.04" \\ "1.18" \end{pmatrix} \\ \begin{pmatrix} "2.93\times10^{-11}" \\ "1.22\times10^{-7}" \\ "5.33\times10^{-9}" \\ "1.44\times10^{-10}" \end{pmatrix} & \begin{pmatrix} "1.22\times10^{-7}" \\ "2.08" \\ "1.84" \\ "0.326" \end{pmatrix} & \begin{pmatrix} "5.33\times10^{-9}" \\ "1.84" \\ "4.85" \\ "1.69" \end{pmatrix} & \begin{pmatrix} "1.44\times10^{-10}" \\ "0.326" \\ "1.69" \\ "0.901" \end{pmatrix} \\ \begin{pmatrix} "2.48\times10^{-14}" \\ "5.88\times10^{-10}" \\ "4.82\times10^{-11}" \\ "1.92\times10^{-12}" \end{pmatrix} & \begin{pmatrix} "5.88\times10^{-10}" \\ "0.057" \\ "0.0947" \\ "0.0248" \end{pmatrix} & \begin{pmatrix} "4.82\times10^{-11}" \\ "0.0947" \\ "0.467" \\ "0.241" \end{pmatrix} & \begin{pmatrix} "1.92\times10^{-12}" \\ "0.0248" \\ "0.241" \\ "0.19" \end{pmatrix} \end{pmatrix} . \quad \text{(S35)}$$

NumberForm[mf*Q // Flatten, 3][[1]] // Total = 169.99 for 60000 s

Next, for 22 values of time t, the matrix (S35) and its sum were calculated. Fig. S4 shows the graphs of the obtained dependence $Q(t)$.

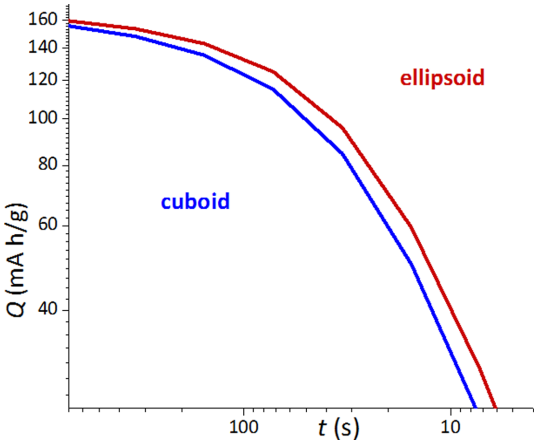

Fig. S4. An example of rate capability calculation for cuboid and ellipsoid crystallite shapes for parameters using 3-dimensional 4-discrete crystallite sizes (S29).

4.2 The influence of discreteness and the importance of taking into account the size distribution of crystallites

For calculations, an HP Laptop 14s, Intel CORE i5-1035G computer was used; with a discreteness of 12, 15, and 24, the calculation time was 45, 90, and 360 minutes, respectively. The situation is quite acceptable for using the developed program with discreteness < 15. However, it is necessary to estimate the magnitude of the error using discreteness and the need, in principle, to use the procedure for determining the parameters of the 3D crystallite size distribution function. The latter can be verified using, in particular, only the mean sizes of the distributions, i.e., assuming the discreteness equal to one, which was used in the calculations of Fig. S5 dependencies.

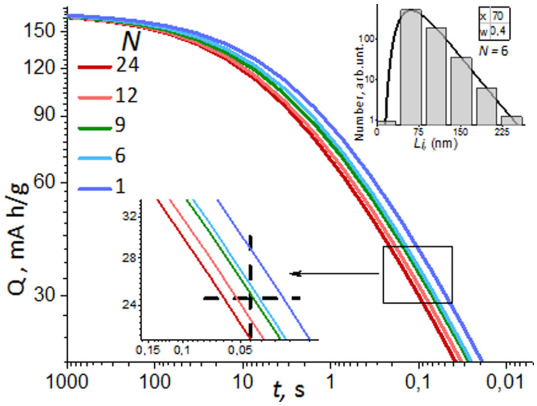

Fig. S5. Dependence of the rate capability on the discreteness of calculations N. The upper inset shows an example of placing discrete points (N=6) on lognormal distributions of ellipsoidal crystallites with average sizes $\bar{L}_i$ = 70 nm, variances σ_i = 0.4, correlation coefficients r_{ij} = 0.5. The lower inset shows an increase in dependences; the discretization error was estimated along the dotted lines.

Fig. S5 shows that the error

1) not using the dispersion of crystallites by size is significant, for the rate capability the error is about 70% more than the value obtained with the discreteness N = 24, for time it is 5 times more;
2) the error depends monotonically on N;
3) for N > 12, the error for the rate capability is < 10%, for time it is < 30%.

Thus, the developed program makes it possible to control and check the results of calculations at intermediate stages of calculations, and to evaluate their errors.

5. Shape engineering is based on the influence of the shape and statistics of crystallites to raise the rate capability

To increase the capacity of $LiFePO_4$ cathodes, efforts are mainly directed to the development of technology (shape engineering) to reduce the size of crystallites along the direction of Li diffusion, along the [010] axis, up to giving them plate and bar shapes. The approach developed in this work makes it possible to quantitatively describe these and other technological experiments.

5.1 Influence of diffusion and electrical relaxation times

From Fig. S6a, it can be seen that at large D the capacitance rate depends to a large extent on the magnitude of the electrical relaxation time with a slope $\eta = 1.0$. Whereas from Fig. S6c it can be seen that for a small value of D, the capacitance velocity depends to a much lesser extent on it with a slope $\eta = 0.5$.

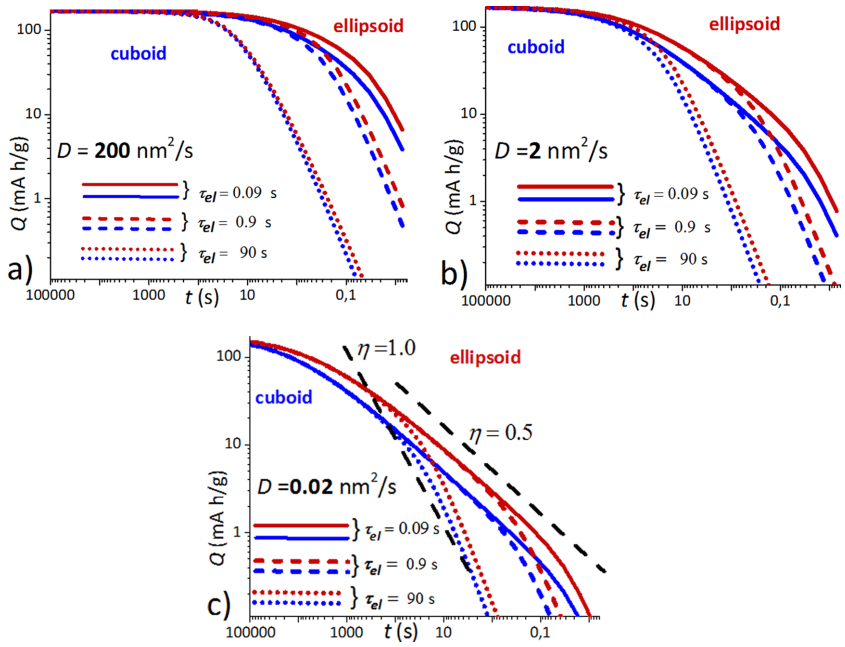

Fig. S6. Capacity rate for three dispersion electrical relaxation times and three diffusion coefficients for cuboids and ellipsoids. Dotted black straight lines are tilted angles in double logarithmic coordinates.

5.2 Influence of face area (010)

The examples of the prevailing plane ac compared to bc for dimensions $\bar{L}_1 \times \bar{L}_2 \times \bar{L}_3$ equal to 15×150×150 and 150×15×150 nm^3, respectively, shown in Fig. S7 and the corresponding dependences in Fig. S8. Here, it turns out to be significant also for small values of τ_{el}.

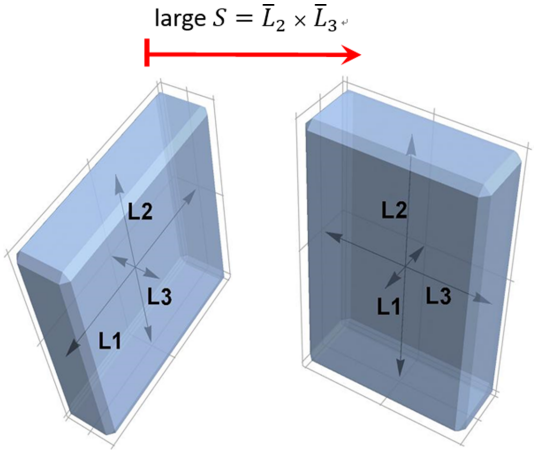

Fig. S7. Examples of cuboids to illustrate two extreme situations with small (left) and big (010) faces

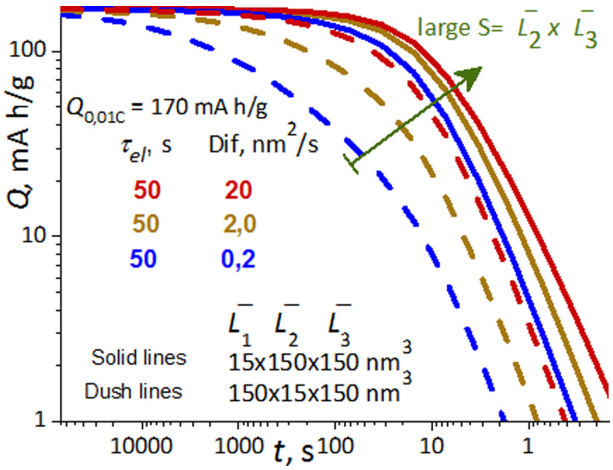

Fig. S8. Capacity rate dependences for the two extreme ratios between the case of perpendicularity of the [010] axis to the dominant face of crystallites (solid lines) and the case when this axis lies in it (dash lines)

6. General case using Lamé curves and superellipses

Known classes of ellipse-like curves, now known as Lamé curves or superellipses, which is defined by the equation [1]:

$$\left(\frac{x}{a}\right)^g + \left(\frac{y}{b}\right)^g = 1 \text{ , (S36)}$$

where shape parameter g is any positive real number.

In our case, superellipsoids are an internal volume bounded by the inequality

$$\left(\frac{2x_1}{L_1}\right)^g + \left(\frac{2x_2}{L_2}\right)^g + \left(\frac{2x_3}{L_3}\right)^g \le 1 \text{ . (S37)}$$

For $g = 2$ and 4, the terms ellipsoid and superellipsoid, respectively, are widely used to denote their shape, and for $g \ge 12$, the shape will be close to a cuboid with an error of less than 1%. Their volume can be calculated by the formula

$$V = \frac{1}{3}L_1L_2L_3\frac{1}{g_2}\beta\left(\frac{1}{g},\frac{1}{g}\right)\beta\left(\frac{2}{g},\frac{1}{g}\right), \text{(S38)}$$

where β- is the beta function.

For column length M_1 in (S24) we have

$$M_1 = \left(\left(\frac{L_1}{2}\right)^g - \left(\frac{L_1}{L_3}x_3\right)^g - \left(\frac{L_1}{L_2}x_2\right)^g\right)^{\frac{1}{g}}, \text{(S39)}$$

and for the region of integration in (S26)

$$reg = \text{ImplicitRegion}[((x\times 2)/L2)^g + ((y\times 2)/L3)^g \le 1, \{x, y\}]; \text{(S40)}$$

Fig. S9 shows several calculations to illustrate the use of equations (S39,S40)

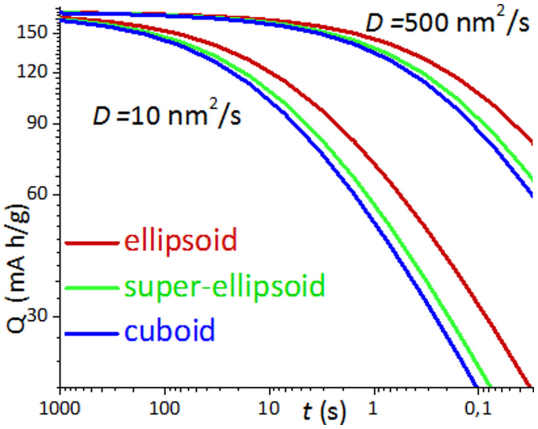

Fig. S9. Rate capacity dependences for g = 2, 4 and 20, shape parameters for ellipsoid, super-ellipsoid and cuboid, respectively.

From Fig. S9, it can be seen that the curve for the superellipsoid is close to the curve for the cuboid, which is largely due to the relatively small difference in their volumes, about 7%, compared with the difference in the volume of the ellipsoid in relation to the volume of the cuboid, about 20% [2].

References

[1] Gabriel Lamé, https://en.wikipedia.org/wiki/Gabriel_Lam%C3%A9
[2] J. W. Bullard and E. J. Garboczi, *Powder Technol.*, **2013**, *249*, 241-252.

7. Three-electrode cell schematic diagram

The three-electrode cell schematic diagram is similar to the classical ones for electroanalytical measurements [1]. The schematic of the cell in application to our problem is illustrated in the Fig. S10.

By a half-cell we mean a cell whose polarizing circuit consists of the electrode under study (*working* electrode, in our case the $LiFePO_4$ composite on aluminum plate) and the *counter* electrode (in our case the lithium metal on a perforated Ti substrate). The measuring circuit includes a separate third electrode. The material of this reference electrode in our case is also lithium.

Our task is to precisely control the current and potential of the working electrode at the same time. The *counter* electrode is polarized, and the controlled current flows through it and the working electrode. But the potential of the counter electrode is unknown because of its polarization. To avoid uncertainty, we introduce a

separate electrode to measure the potential. No current flows through it, it is not polarized, and its potential is strictly defined. This is the *reference* electrode. We measure the potential of the working electrode relative to it.

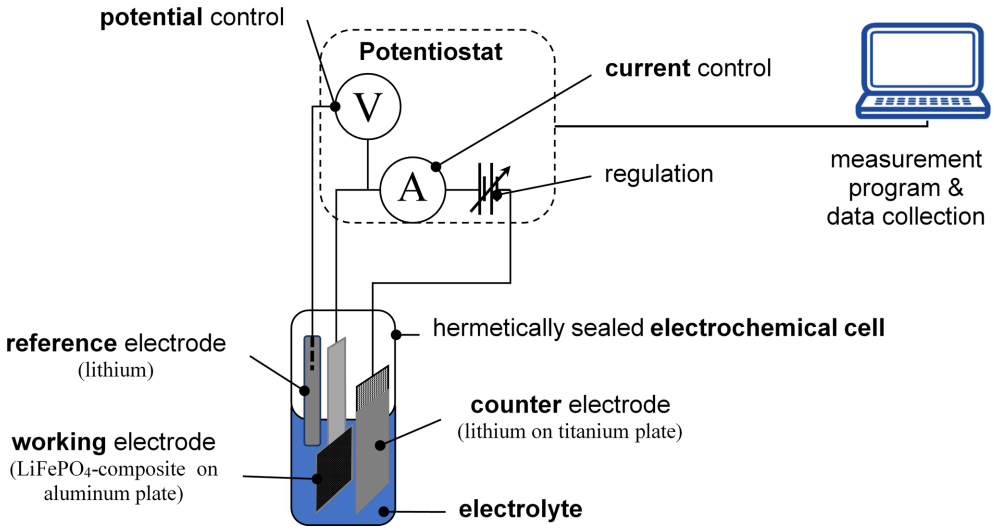

Fig. S10. Schematic of the electrochemical measurement in three-electrode cell

References

[1] F. Scholz (Ed.), *Electroanalytical methods: Guide to experiments and applications*, 2nd ed., Springer, Berlin, **2010**.